Flat-plate boundary-layer transition in hypersonic flows

By C. Stemmer

1. Motivation and objective

Knowledge on transitional flows at elevated Mach numbers is very limited due to the immense difficulty in conducting experiments – be it wind-tunnel or free-flight. Therefore, direct numerical simulation provides a very powerful tool to gain significant insight into these high-temperature flows. These high-temperature hypersonic flows become chemically reacting creating additional challenges for the modeling of chemical reactions and the thermodynamic properties of such flows. The simulation of laminar-turbulent transition in boundary-layer flows for entry scenarios can deliver estimates of flight-relevant physical properties such as drag and heat transfer important for the flight path design and the design of the heat shield of an entry vehicle, respectively.

Early efforts to investigate hypersonic flows involved rockets in free-flight experiments, where qualitative results where obtained for the transition location (see Schneider (1999)). These experiments, according to Schneider, are not very reliable in terms of quantitativeness since the angle of attack is not measured accurately enough. Recent efforts to investigate hypersonic flows include Ma=21 experiments by a Russian group, Mironov & Maslov (2000), at Novosibirsk, which can serve as a qualitative comparison to the presented direct numerical simulations. Free-flight hypersonic experiments are not to be expected in the near future due to the sheer cost involved.

Direct numerical simulations with high-order finite-difference schemes shall be employed to unveil some of the important mechanisms in the evolution of laminar-turbulent transition in flat-plate boundary-layer flows. The differences between transition assuming ideal-gas and chemically-reacting flows is the main goal of this ongoing investigation.

2. Numerical method

The well-documented numerical method developed by Adams (1996), Adams (1998) and Adams (2000) for turbulent compression-ramp flow is employed for the high Mach-number simulations. The discretization is on the base of the conservative, compressible Navier-Stokes equations. The mesh is uniform in the downstream direction and variable in the wall-normal direction allowing for the collocation of grid points at the boundary-layer edge. The numerical method is a compact one and sixth-order accurate in space with periodic boundary conditions in the spanwise direction. The time advancement is done with a Runge-Kutta time integration scheme of third order accuracy. Very sharp gradients that cannot be resolved through the numerical scheme are captured in all three spatial directions through a hybrid ENO-scheme singling out the regions where it needs to be applied only. For the incorporation of the chemical and thermal high-temperature effects, the modeling of Stemmer & Mansour (2001) is used.

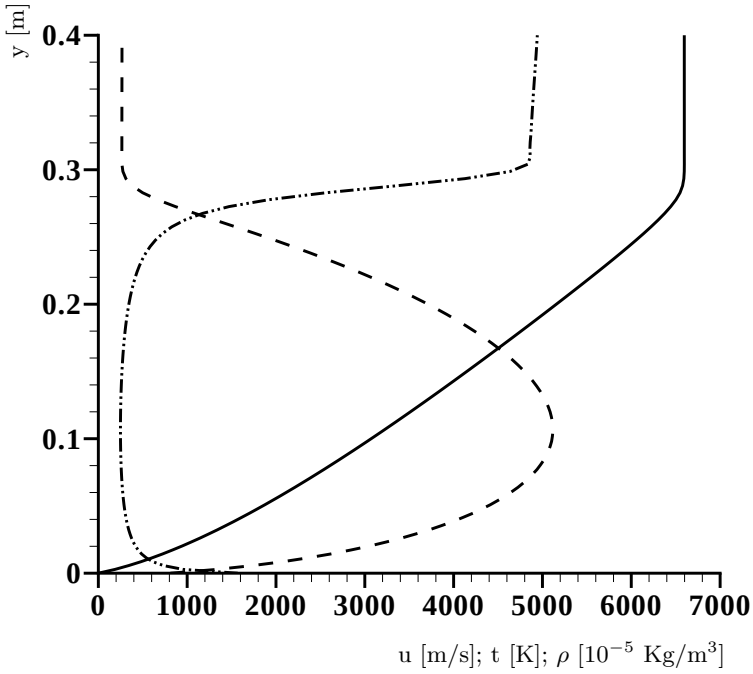

FIGURE 1. Wall-normal profiles of streamwise-velocity, temperature and density for Re_x=4 $\cdot 10^6$ in dimensional units. Note that the density has been multiplied by a factor of 10^5 to show on the graph.

Disturbances are introduced at the wall through a disturbance strip. Blowing and suction is applied simultaneously to ensure that zero net mass is introduced at any one time step (see Eißler, (1995))

$$(\rho v)|_{wall} = Ag(z,t)\frac{81}{16}\zeta^3(3\zeta^2 - 7\zeta + 4), \qquad 0 \le \zeta \le 1,$$
$$(\rho v)(2-\zeta)|_{wall} = -A(\rho v). \tag{2.1}$$

The function $g(z,t)$ is a trigonometric function in time and space.

The dimensional quantities of the Ma=20 flow at free-stream conditions at an altitude of H=50km are U_∞=6596 m/s, $\rho_\infty = 1.027{\cdot}10^{-3}$ Kg/m^3, $T_\infty = 270.65$ K and the viscosity is $\mu_\infty = 1.703{\cdot}10^{-5}$ Kg/(m$\cdot$ s) according to the US Standard Atmosphere (1976). An isothermal case is investigated with $T_{wall} = 3T_\infty = 811.95$ K .

The ideal gas boundary layer equations, Anderson (1989), were solved for the starting solution of the base-flow calculations. The wall-normal profiles of downstream velocity (u), temperature (t) and density (ρ) are shown in figure 1. The sharp rise in density at the boundary-layer edge (y=0.29 m) is a prominent feature of the boundary-layer profiles, which underlines the necessity of a fine resolution at that wall-normal position.

For the present simulation, a resolution of 1500 x 240 x 6 points in x, y and z-direction are used. This yields a resolution of $\Delta x = 0.066$, $\Delta y_{min} = 7.717 \cdot 10^{-3}$ and $\Delta z = 0.146$, where the lengths are made dimensionless with the boundary-layer thickness $\delta_1 =$ 0.2197m.

In deviation to the ideal gas case, vibrational degrees of freedom were incorporated in the code for the calculation of the thermodynamic properties.

3. Stability properties

After Lees & Lin (1946) had laid the foundation of a compressible stability theory through an asymptotic viscous approach, Mack (1969) developed the full parallel theory for finite Reynolds numbers. The stability properties are evaluated through linearization of the complete Navier-Stokes equations in a locally parallel flow. The disturbances are assumed to be harmonic in nature

$$q'(x,y,z,t) = q(y)\exp\left[i(\alpha x + \beta z - \alpha c t)\right], \tag{3.1}$$

where q={u,v,w,ρ,p,t}. The wave numbers α and β are complex in the most general sense and describe temporal as well as spatial growth. The reader is kindly referred to Gaster (1965) for the transformation of spatial amplification rates into temporal amplification rates and vice versa.

Mack's original computer code for ideal-gas flows was available to produce the presented stability results for the Ma=20 flow. Mack normalizes the stability results with the Reynolds number defined as

$$R_x = \sqrt{Re(x)} = \sqrt{\left(\frac{\tilde{\rho}\tilde{U}\tilde{x}}{\tilde{\mu}}\right)}, \tag{3.2}$$

where variables with a tilde denote dimensional variables. The wall-normal coordinate $\tilde{y}$ is non-dimensionalized through

$$\eta = \tilde{y}\cdot\frac{R_x}{\tilde{x}}. \tag{3.3}$$

The boundary-layer thickness for this case is $\eta(\delta) \approx 29.1$.

The frequency parameter F is defined as $F=\tilde{f}2\pi\tilde{\mu}/(\tilde{\rho}\tilde{U}^2)$. For the dimensionless frequency of $F=3.6416\cdot10^{-5}$, the dimensional frequency is $\tilde{f}$ = 15.2 KHz. Firstly, two-dimensional disturbances are investigated since they turn out to be the most amplified waves for the chosen frequency. The spatial amplification rate $-\alpha_i$ over a wide range of Reynolds numbers is shown in figure 2 compared to two-dimensional disturbances with a slightly higher frequency. For the higher frequency, the same pattern appears but is shifted to smaller Reynolds numbers R_x. Two local peaks of the spatial amplification can be identified at $R_x \approx 1000$ and $R_x \approx 2250$. Comparing the eigenfunctions for the pressure p at these respective Reynolds numbers, one can identify the first peak with a first mode disturbance (according to the classification by Mack). At these high Mach numbers, the areas of instability merge and the amplification rate shows unstable waves as the eigenfunctions switch to a second mode disturbance. The peak at $R_x \approx 2250$ is associated with such a disturbance exhibiting a zero in its wall-normal amplitude profile. The number of zeros is one less than the mode number given by Mack. At $R_x \approx 3500$, the third mode is present with a slightly lower peak in the amplification rates. Downstream of $R_x \approx 4000$, the two-dimensional disturbance will encounter damping as the amplification rate $-\alpha_i$ becomes negative for this frequency.

The phase velocities of the unstable eigensolution is shown in figure 3. Inviscid theory predicts a phase speed of $c_{ph} = 1 - \frac{1}{Ma} = 0.95$ which is very close to the observed phase velocities of $c_{ph} \approx 0.98$ which in turn is very close to the free-stream velocity. Every peak in the spatial amplification rates coincides with a local minimum in the phase velocities.

Wall-normal profiles of the eigensolutions of the stability problem are shown at the local Reynolds number of R_x= 1000 (first mode disturbance) in figure 4. This two-dimensional mode represents the first peak in figure 2. The eigenfunctions of the downstream velocity

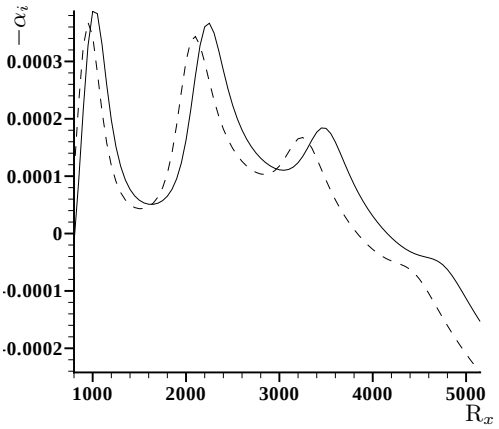

FIGURE 2. spatial amplification rates $-\alpha_i$ vs. the downstream direction for two-dimensional disturbances at F=3.6416·10^{-5} (———) and F=3.9·10^{-5} (- - - -)

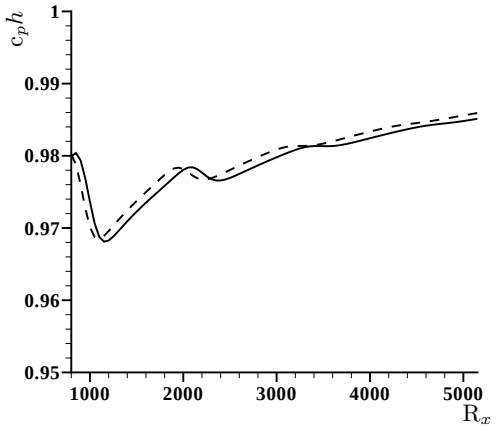

FIGURE 3. phase velocity $c_p h$ vs. the downstream direction for two-dimensional disturbances at F=3.6416·10^{-5} (———) and F=3.9·10^{-5} (- - - -)

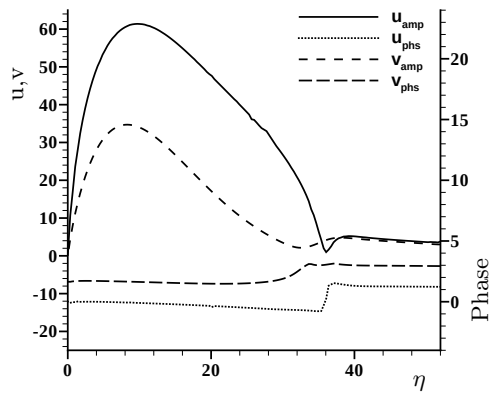

FIGURE 4. u and v eigensolutions at R_x=1000 for two-dimensional disturbances at F=3.6416·10^{-5}. u_{amp} (———), v_{amp} (- - - -), u_{phs} (·····), v_{phs} (— — —).

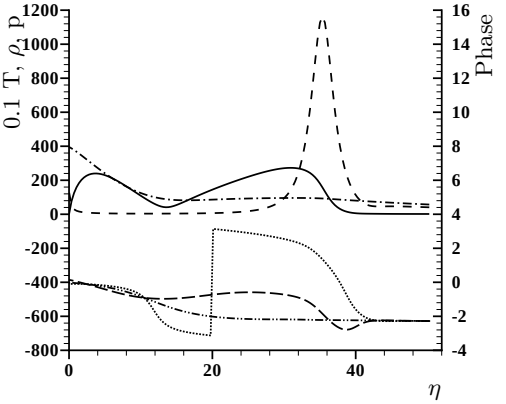

FIGURE 5. t, ρ and p eigensolutions at R_x=1000 for two-dimensional disturbances at F=3.6416·10^{-5}. t is scaled by a factor of 0.1. t_{amp} (———), ρ_{amp} (- - - -), p_{amp} (—·—), t_{phs} (·····), ρ_{phs} (— — —), p_{phs} (—··—).

u and the wall-normal velocity v both show a distinct maximum inside the boundary layer and a second, much smaller maximum outside the boundary layer typical for the first mode disturbance. The pressure (see figure 5) has no zero in it's profile distinguishing the first mode eigenfunction.

At the local Reynolds number of R_x= 2450, the second mode disturbance is the most unstable eigenmode. The wall-normal profiles of the eigensolutions of the stability equations are shown in figure 6 and 7. For higher Mach-numbers, the second mode is generally strongly amplified. For the high Mach number chosen, the amplification rates of the two-dimensional first and second modes are very close.

In figure 6, the eigenfunctions for the downstream velocity u and the wall-normal ve-

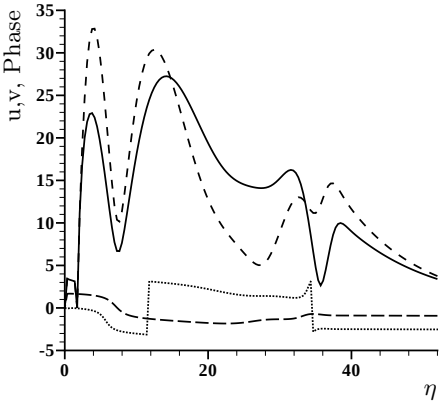

FIGURE 6. u and v eigensolutions at R_x=2450 for two-dimensional disturbances at F=3.6416·10^{-5}. u_{amp} (———), v_{amp} (- - - -), u_{phs} (·····), v_{phs} (— — —).

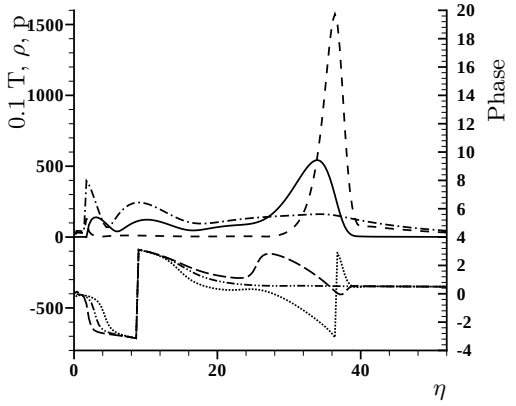

FIGURE 7. t, ρ and p eigensolutions at R_x=2450 for two-dimensional disturbances at F=3.6416·10^{-5}. t is scaled by a factor of 0.1. t_{amp} (———), ρ_{amp} (- - - -), p_{amp} (—·—), t_{phs} (·····), ρ_{phs} (— — —), p_{phs} (—··—).

locity v are shown together with their phase distribution for that local Reynolds number. Compared to the earlier station R_x= 1000 (figure 4), the eigenfunctions now show a double peak inside the boundary layers. As one goes further downstream (not shown here), the number of maxima inside the boundary layer increases. The pressure as shown in figure 7 shows a phase shift of π at η=4 identifying the second mode. It can be noted, that the density eigenfunction looks almost identical to the case at R_x= 1000.

The results for the third mode at R_x = 2800 will be shown together with the simulation results further into the report.

The importance of the three-dimensional modes for the above described conditions is discussed by means of figure 8 showing the dependence of the amplification rate on the obliqueness angle of the disturbance φ. Four downstream locations are shown. For R_x= 800, before the first-mode instability sets in, there is almost no dependence on the obliqueness angle for the damped waves. As the first-mode instability is at its peak at R_x= 1000, low obliqueness waves are almost as unstable as the two-dimensional disturbance up to approximately 20°. The amplification rates drops continuously down to neutral at about φ= 65°. For R_x= 2250, the picture is very similar to the station where the first-mode instability is at its maximum.

The presented stability results are based on a non-reacting ideal-gas flow. The effects of the chemical reactions have been studied among others by Johnson, Seipp & Candler (1998), which have found that chemical reactions can diminish amplification rates and delay transition. This coincides with other work on chemically reacting flow.

4. Results

The simulations have been carried out under free-flight conditions at an altitude of H=50 Km (compare page 390 for the dimensional properties). The disturbances were introduced at a Reynolds number of R_x = 2250 (x=58). An acoustic disturbance is introduced which propagates towards the upper boundary at the Mach angle of $\theta \approx 3°$. This accounts for the elevated amplitudes in the presented results for $y > 0.3$.

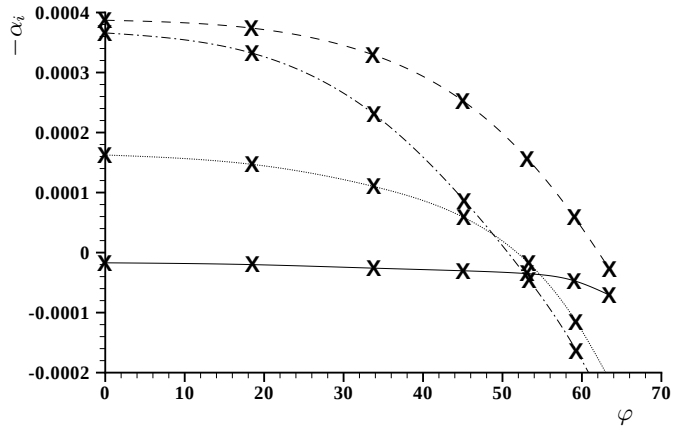

FIGURE 8. spatial amplification rate $-\alpha_i$ vs. wave propagation angle φ for F=3.6416·10^{-5}. R$_x$= 800 (———), R$_x$= 1000 (- - - -) R$_x$= 2000 (·····) R$_x$= 2250 (—·—).

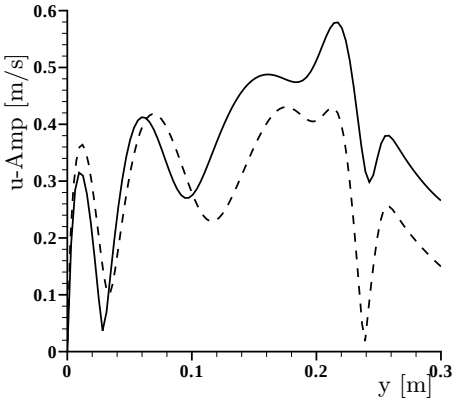

FIGURE 9. Comparison of simulation (———) and Linear Stability results (- - - -) of the downstream velocity u at $R_x = 2800$

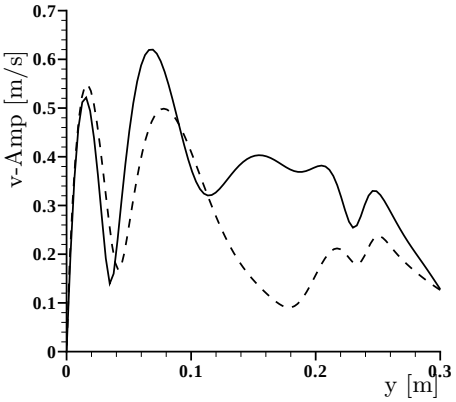

FIGURE 10. Comparison of simulation (———) and Linear Stability results (- - - -) of the wall-normal velocity v at $R_x = 2800$

The results for the most-amplified two-dimensional disturbance are compared with the stability results acquired through Mack's stability code in figures 9-12 at $R_x = 2800$. The downstream velocity (u) in figure 9 shows very close agreement to the theoretical results reproducing the phase shift at the right wall-normal distances. The way the disturbances are introduced opens the possibility of the presence of multiple instability waves with the same frequency but differing wave numbers.

The deviation from the theoretical results can be explained through the inclusion of the vibrational modes in the calculation of the thermodynamic properties. In areas of high temperature (above $\sim$ 3000 K), this will alter the temperature profile compared to the ideal-gas case. This happens at $0.2 < y < 0.3$ for $R_x = 2800$ and can explain the differences there.

The wall-normal velocity (v) is presented in figure 10, pressure (p) and density (ρ) are

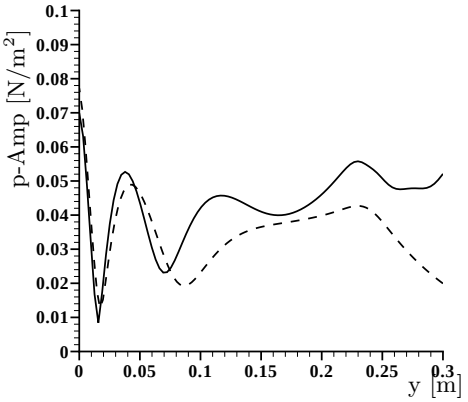

FIGURE 11. Comparison of simulation (———) and Linear Stability results (- - - -) of the pressure p at $R_x = 2800$

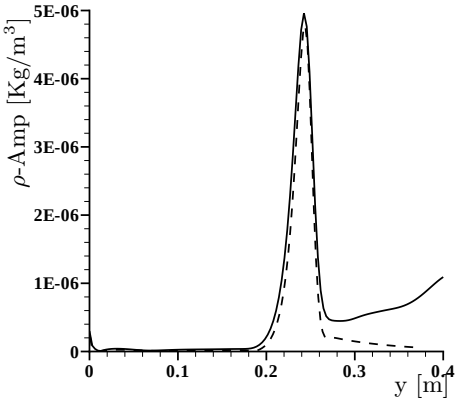

FIGURE 12. Comparison of simulation (———) and Linear Stability results (- - - -) of the density ρ at $R_x = 2800$

shown in figure 11 and figure 12, respectively. The temperature results are qualitatively the same as the presented results.

The amplification rate given by the stability theory results is $\alpha_i = -0.0186[1/m]$ and the rate obtained from the simulation is $\alpha_i = -0.017[1/m]$.

5. Conclusions and future work

It has been shown that the numerical method presented is capable of tackling the hypersonic transition problem proposed. The results of the Linear Stability Theory match well with the simulation results for a third mode unstable two-dimensional disturbance.

Fundamental and oblique transition scenarios for the described Ma=20 flow will be performed. Simulations will be undertaken to provide for chemical and thermal non-equilibrium conditions.

To mimic closer the introduction of disturbances in an experimental environment, a point source disturbance, Stemmer (2001), will be introduced. Therefore, a single frequency with all possible spanwise wave numbers can be excited simultaneously leaving the flow to naturally amplify the unstable components of the disturbance.

Laminar-turbulent transition scenarios under varying disturbance conditions will be investigated to understand more about the physical behaviour of chemically reacting flows in transition on a flat plate.

REFERENCES

Adams, N. A. 1996 A high-resolution hybrid compact-ENO scheme for shock-turbulence interaction problems. *J. Comp. Phys.* **127**, 27-51.

Adams, N. A. 1998 Direct numerical simulation of turbulent compression ramp flow *Theor. and Comp. Fluid Dyn.* **12**, 109-129.

Adams, N. A. 2000 Direct simulation of the turbulent boundary layer along a compression ramp at M=3 and Re_θ=1685. *J. Fluid. Mech.* **420**, 47-83.

Anderson, J. D. 1989 *Hypersonic and high temperature gas dynamics.* AIAA publication.

Blottner, F. G., Johnson, M. & Ellis, M. 1971 *Chemically reacting viscous flow program for multi-component gas mixtures.* Sandia Natl. Laboratories, SC-RR-70-754.

Eissler, W. 1995 *Numerische Untersuchungen zum laminar-turbulenten Strömungsumschlag in Überschallgrenzschichten.* Dissertation, Universität Stuttgart.

Gaster, M. 1965 A note on a relation between temporally increasing and spatially increasing disturbances in hydrodynamic stability. *J. Fluid. Mech.* **22**, 222-224.

Hirschfelder, J. O., Curtiss, C. F. & Bird, R. A. 1964 *Molecular theory of gases and liquids.* Wiley, New York.

Johnson, H. B., Seipp, T. G. & Candler, G. V. 1998 Numerical study of hypersonic reacting boundary layer transition on cones *Physics of Fluids.* Vol. **10**, 2676-85.

Lees, L. & Lin, C. C. 1945 *Investigation of the stability of the laminar boundary layer in a compressible fluid.* NACA TN 1115.

Mironov, S. G. & Maslov, A. A., 2000 Experimental study of secondary stability in a hypersonic shock layer on a flat plate. *J. Fluid. Mech.* **412**, 259-277.

Mack, L.M., 1969 *Boundary-layer stability theory.* JPL Report 900-277 Rev. A, Jet Propulsion Laboratory, Pasadena, USA.

Park, C. 1989 A review of reaction rates in high temperature air. *AIAA Paper 89-1740.*

Sarma, G. S. R. 2000 Physico-chemical modeling in hypersonic flow simulation. *Prog. Aerospace Science* **36**, 281-349.

Schneider, S. P. 1999 Flight data for boundary-layer transition at hypersonic and supersonic speeds. *J. of Spacecraft and Rockets* **36**, 8-20.

Stemmer, C. 2001 *Direct numerical simulation of harmonic point source disturbances in an airfoil boundary layer with adverse pressure gradient.* Dissertation, Universität Stuttgart.

Stemmer, C. & Mansour, N.N. 2001 DNS of transition in hypersonic boundary-layer flows including high-temperature gas effects. *Annual Research Briefs 2001*, Center for Turbulence Research, NASA Ames/Stanford University., 143-150.

Stuckert, G. K. & Reed, H. L. 1991 Unstable branches of a hypersonic, chemically reacting boundary layer. *Boundary Layer Transition and Control*; Proceedings of the Conference, Univ. of Cambridge, UK, Apr. 8-12, 1991, 19.1-19.13.

U.S. Standard Atmosphere, U.S. Government Printing Office, Washington, D.C., 1976.

Vincenti, W. G. & Kruger. C. H. 1982 *Introduction to physical gas dynamics.*, Krieger, Malabar, FL.

Wilke, S. P. 1950 A Viscosity equation for gas mixtures. *J. Comp. Phys.* **18**, 517-519.